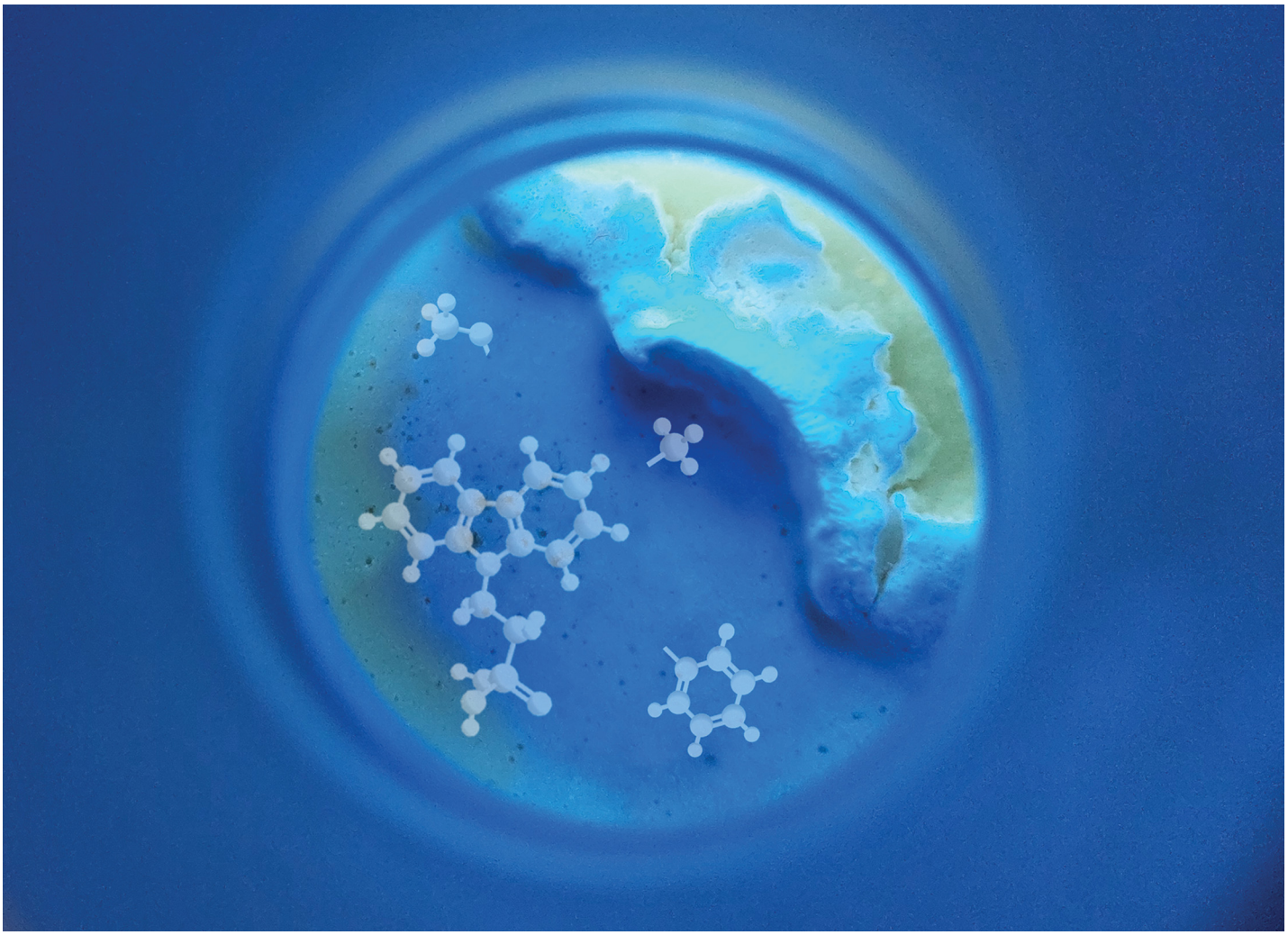

Showcasing research from Kaunas University of Technology (KTU), Lithuania in collaboration with Helmholtz-Zentrum Berlin (HZB).

Screening of the carbazole-based phosphonic acids in perovskite solar cells: impact of the substitution pattern on device performance

This work presents a comparative study of nine carbazole-based phosphonic acids used as self-assembled monolayers (SAMs) in p–i–n perovskite solar cells. By varying methyl, methoxy, and phenyl substituents at different positions, the study reveals that molecules substituted at the 3,6-positions achieve the highest fill factors and improved charge extraction, supported by trSPV and PESA analyses. A threshold ionization potential of ~5.45 eV was identified, beyond which device performance declines. This work provides insightful knowledge that can contribute to further investigations and design of phosphonic acid-based materials.

Image reproduced by permission of Aida Drevilkauskaitė from *Mater. Adv.*, 2025, **6**, 8921.

As featured in:

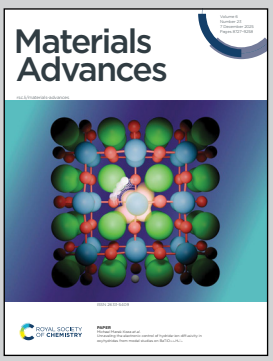

See Artiom Magomedov *et al.*, *Mater. Adv.*, 2025, **6**, 8921.

ROYAL SOCIETY OF CHEMISTRY

rsc.li/materials-advances

Registered charity number: 207890

Materials Advances

ROYAL SOCIETY OF CHEMISTRY

PAPER

View Article Online
View Journal | View Issue

Cite this: *Mater. Adv.*, 2025, **6**, 8921

Screening of the carbazole-based phosphonic acids in perovskite solar cells: impact of the substitution pattern on device performance

Aida Drevilkauskaitė, [a] Lea Zimmermann, [b] Isabella Taupitz, [b] Sergei Trofimov, [c] Boris Naydenov, [c] Eike Köhnen, [b] Vytautas Getautis, [a] Steve Albrecht [b] and Artiom Magomedov *[a]

Self-assembled monolayers (SAMs) have become the standard hole-selective layer in high-efficiency p–i–n perovskite single-junction and multi-junction solar cells. Since there is limited information about the structure–property correlation, it is important to determine how structural changes in the molecule impact performance or enhance layer properties. In this work, nine different carbazole-based phosphonic acids with methyl, methoxy, and phenyl functional groups were compared to investigate the correlation between the chemical structure and device performance. The results reveal that phosphonic acids with different functional groups share some structure–property correlations and that substituents at 3,6 positions (**3,6-Me-2PACz**, **3,6-Ph-PACz**, and **3,6-MeO-2PACz**) of carbazole have higher perovskite single-junction device fill factors, which is one of the factors determining the performance of the device, than molecules with substituents in 2,7 or 4 positions. These findings were supported by transient surface photovoltage (trSPV) measurements. In addition, correlation between ionisation potential and fill factor suggests the threshold value, after which the fill factor is reduced, possibly due to the energy level misalignment. Additionally, the impact of different functional groups in the molecule was investigated with optical, thermal, and electrophysical methods by combining experimental and simulation methods. This work provides insightful knowledge that can contribute to further investigations and design of phosphonic acid-based materials.

Received 3rd July 2025,
Accepted 1st October 2025

DOI: 10.1039/d5ma00703h

rsc.li/materials-advances

Introduction

The perovskite solar cell (PSC) technology is currently on the way from lab to fab, demonstrating rapid progress in terms of efficiency and up-scaling.[1] This process is closely related to the advancements in the development of new materials. In particular, the introduction of so-called "self-assembled monolayers" (SAMs) as hole-selective layers (HTLs) in the p–i–n (or "inverted") PSCs was one of the major breakthroughs, shaping the field.[2] Since their introduction in 2018[2,3] 2PACz ([4-(9*H*-carbazol-9-yl)butyl]phosphonic acid) and related materials with various functional groups have been used in most of the record-achieving perovskite/Si tandem solar cells[4–7] as well as the most efficient single-junction PSC.[8] The main factor that led to their widespread use is a combination of (i) high efficiencies due to the low non-radiative recombination and efficient charge extraction at the SAM-perovskite interface,[3] (ii) compatibility with various deposition methods (*e.g.* dip-coating, spin-coating, blade coating, and vapor deposition),[9] (iii) the broad processing window which allows optimization within a wide range of processing conditions, making it easy to use these compounds, and (iv) broad availability of these materials from commercial sources.

The basic design of the SAM molecules combines two functionalities – the anchoring group and the semiconducting fragment. As an anchoring group, phosphonic acid is the common choice for functionalization of various oxides, such as ITO (indium-tin oxide).[10–13]

Due to the presence of phosphonic acid, strong binding occurs on the metal oxide surface, potentially leading to a layer with the thickness of a single molecule. It can be expected that such a simple molecular design, combined with the orientation of the molecules, should enable the rational design of the target compounds. However, there is a lack of a general picture of the processes taking place at the microscopic level. In such a

[a] *Department of Organic Chemistry, Kaunas University of Technology, Radvilenu pl. 19, Kaunas, 50254, Lithuania. E-mail: artiom.magomedov@ktu.lt*
[b] *Helmholtz-Zentrum Berlin für Materialien und Energie, Division Solar Energy, Kekulestraße 5, 12489 Berlin, Germany*
[c] *Department Spins in Energy Conversion and Quantum Information Science (ASPIN), Helmholtz-Zentrum Berlin für Materialien und Energie, Hahn-Meitner-Platz 1, 14109 Berlin, Germany*

situation, when the underlying fundamental processes are not fully understood and are difficult to access experimentally, screening methods can be applied. This can provide a general structure–property relationship, suggesting the path towards further optimization of the chemical structure.

While the screening method has its advantages, so far, the vast majority of studies have been limited to 2 or 3 materials, because device fabrication and optoelectronic characterization remain labor and time intensive, and researchers tend to prioritize maximizing champion performance over systematic benchmarking.[14] Moreover, comparing materials that were tested in PSCs can be challenging due to the variations in electronic properties and preparation techniques of the absorber layer.

Additionally, the device structure and equipment or methods used to make the device vary across different institutions. This can further impact the performance of the final device and limit comparability.

With this work, we aim to provide the first comparison of the larger set of nine phosphonic-acid-based molecules, comparing their performance in the same model PSC system, including previously published (**2PACz**, MeO-2PACz (**3,6-MeO-2PACz**), Ph-PACz (**3,6-Ph-2PACz**), Me-2PACz (**3,6-Me-2PACz**) and DC-PA (**2,7-MeO-2PACz**)), and the new compounds (**4-Ph-2PACz**, **2,7-Ph-2PACz**, **4-MeO-2PACz**, **2,7-and Me-2PACz**) where names provided in bold are used throughout the text for consistency and clarity, and full chemical names are given in the SI.[3,15–17]

Results and discussion

Synthesis and choice of materials

The reference material that was used in this work was **2PACz**. Currently, **2PACz** represents the SAM material with the most simplistic chromophore, which is connected to the phosphonic acid anchoring group through the ethylene linker. For the investigated compounds we have chosen to keep the length of the linker fragment the same as in **2PACz** and **3,6-MeO-2PACz**, to have a direct comparison. In addition, previous studies showed that shorter spacers can lead to higher values of photovoltaic parameters, denser packing, and stronger intermolecular interactions.[18,19]

To study the influence of the carbazole substitution pattern, when functional groups are connected to the carbazole core at the positions highlighted on the **2PACz** molecule in Fig. 1, three common functional groups (methyl, phenyl, and methoxy) were selected. The first two, methyl and phenyl functional groups were previously used in the devices with high fill factor (FF) with over 82% in wide bandgap perovskites (1.67–1.68 eV),[7,17] while methoxy is popular in highly efficient structures with 1.53–1.55 eV bandgap perovskite.[20,21]

Simple and synthetically accessible materials were chosen as a study object, aiming to empirically demonstrate the influence of the chemical substitution patterns on the performance of the final devices. Following the established procedures of previous reports, phosphonic acid and linker fragments were introduced *via* alkylation, Arbuzov reaction, and nucleophilic cleavage set of reactions as shown in Fig. 2.

Most of the chromophores were obtained from commercial sources or synthesized (in the case of 4-methoxy-9*H*-carbazole). A detailed description of the synthesis, and purification protocols, as well as analysis data (NMR, combustion-based CHN elemental analysis), is available in the SI (Fig. S1–S26). Overall, a set of nine materials was prepared for further tests, as shown in Fig. 1, including four previously unpublished compounds.

Properties of the SAM materials and films

To study the properties of the investigated compounds, the materials and their layers (bulk SAM materials and ITO/SAM stack) were characterized by utilizing UV/vis, PL, TGA, DSC, PESA and KPFM techniques. These measurements can act as a support for the analysis of the performances of the devices, as well as provide general information on the properties of these compounds.

First, the optical properties of the synthesized compounds were studied by UV/Vis and photoluminescence spectroscopy (Fig. 3).

Due to the very thin nature of the SAM layer, usually there are no problems associated with parasitic absorption; therefore, UV/Vis is mostly used to reflect the changes in the chromophore system. Materials with phenyl substituents showed broader absorption than compounds with methoxy or methyl groups. The broader absorption can be caused by the increased rotational freedom of phenyl groups in the molecule, which increases conformational flexibility and reduces molecular planarity. Methyl-substituent compounds showed a slight bathochromic shift, possibly due to the electron-donating properties of this group, which lowers the energy required for the electronic transition. A redshift was observed for molecules with substituents in the 3,6 and 2,7 positions, while compounds with functional groups in the 4-position showed a slight blue shift.

Next, we performed thermal gravimetric analysis (TGA) to determine the decomposition temperature (T_{dec}), defined as the point at which the material experiences a 5% mass loss. All thermal gravimetric data is provided in Fig. 3d and SI (Table S1). While the devices are not expected to reach very high temperatures (over 100 °C), for some perovskite compositions, high annealing temperatures of above 100–170 °C might be used.[22] Therefore, TGA was used to investigate the material's stability. In addition, TGA can be used to estimate the possibility of processing materials by the physical vapor deposition (PVD) method, if the drop in weight is fast. The obtained values of the T_{dec} are in the range from 234 °C to 347 °C. Lower T_{dec} might be caused by the removal of water during heating, which can be trapped in the crystalline structure as hydration water,[23] which is expected to be removed during the SAM annealing step in device fabrication. Compounds with methyl and phenyl functional groups showed rapid weight loss in a narrow range of temperatures, suggesting possible sublimation and compatibility with the PVD technique. Methoxy-substituted compounds demonstrated two-step mass reduction, which might

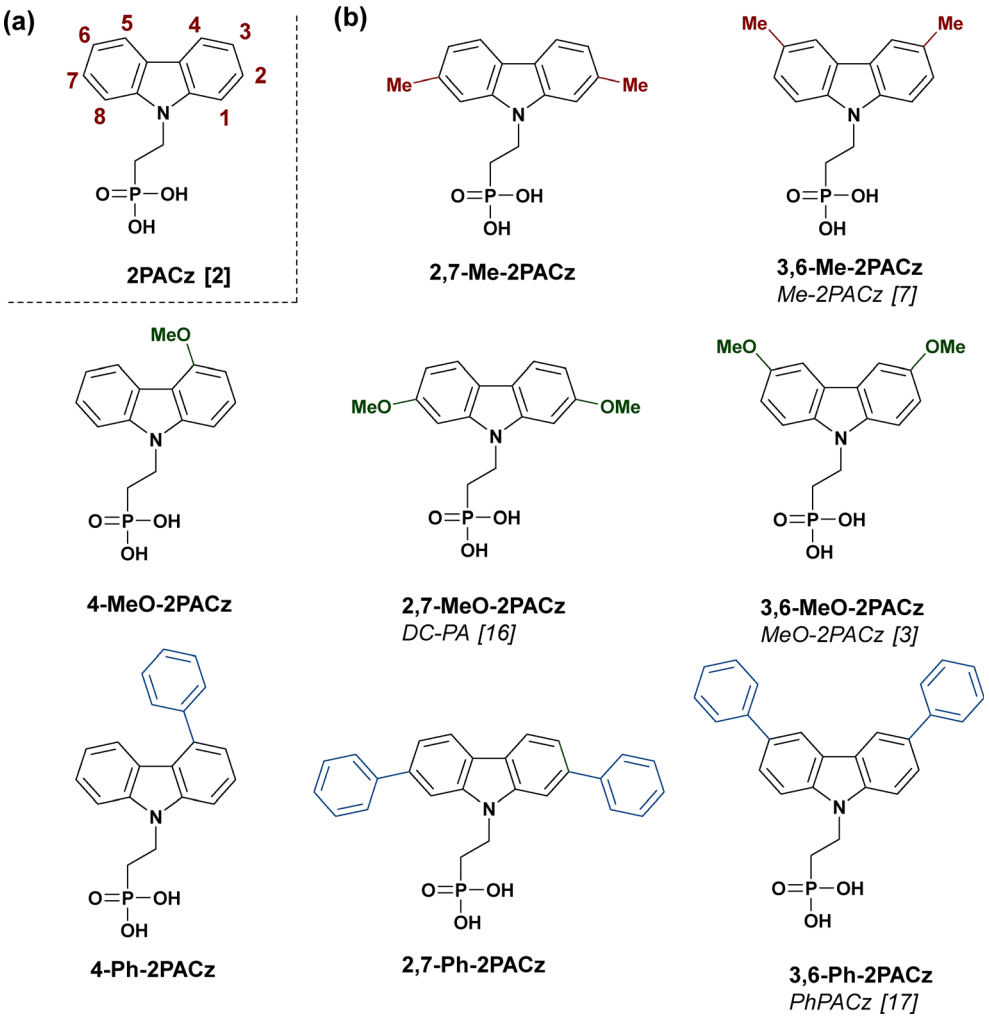

Fig. 1 Structures of investigated SAM molecules. (a) Carbazole-core positions are numbered on the 2PACz molecule and used in this paper as the standard material. (b) Series of materials with Me-, MeO- and Ph-substituents in different positions. For the published compounds, references to previous studies and alternative names are provided in italic.

indicate loss of crystallization water, as well as chemical decomposition.

To additionally test the stability of the materials under elevated temperatures and UV illumination, we have aged the drop-casted samples at 85 °C, 390 nm LED light, N_2 atmosphere. A more detailed description is provided in the SI. As can be seen from Table S4, the variations in ionization potential (I_p) were not significant (<0.1 eV), suggesting good stability of the investigated compounds under such conditions.

In case of **3,6-MeO-2PACz** and **3,6-Ph-2PACz** some increase in the gradient was observed. Such change could be linked to the change in the density of states and/or energetic disorder of the materials.

It is well established that while SAM materials lead to good performance of the devices, there are common problems with surface wettability properties. Therefore, if materials result in similar performances, it is preferred to use ones with better wettability properties. The simplest way to evaluate the wettability is the water droplet method. The samples for this characterization were prepared by depositing a 1 mmol ml^{-1} solution of each PACz material by spin-coating on glass/ITO followed by annealing and washing the surface with ethanol. A 0.01 ml droplet of distilled water was deposited onto the surface using a micro syringe. All measurements were performed at room temperature under ambient conditions, and each sample was measured at multiple points on the same substrate. The contact angles given in Table S2 represent the average values. The water droplet angle on the surface of the different materials varied from 69° to 80°. All the layers showed a higher contact angle than the ITO layer (54°), indicating successful layer formation on top of the surface. As expected, materials with a hydrophobic phenyl group showed an increase in the contact angle value, in comparison with **2PACz**. Materials with the methoxy substituents resulted in lower contact angle values. The highest values were observed in layers with materials substituted at the 4-position of the carbazole core.

One of the important characteristics of the organic semiconductor is the position of its energy levels. For the determination of the energetic levels, several methods can be applied, such as cyclic voltammetry (CV) ultraviolet photoelectron

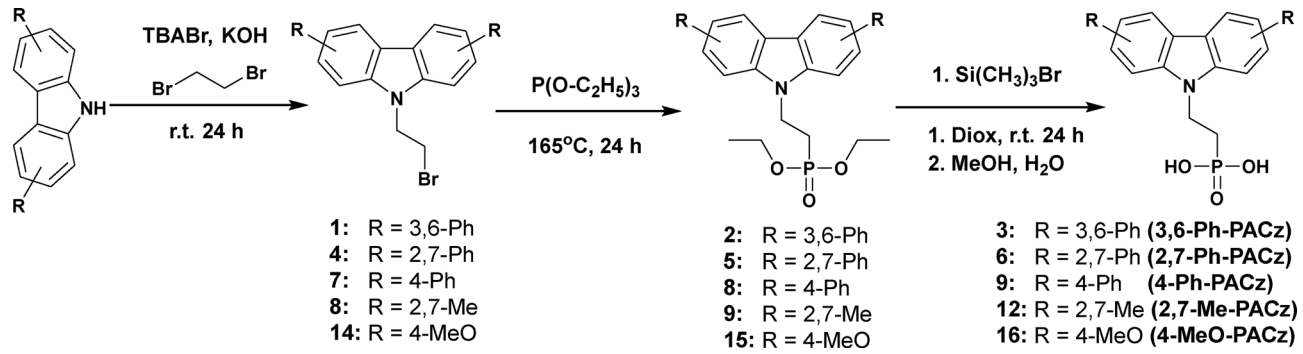

Fig. 2 Synthesis route of SAM molecules with substituents in various positions.

spectroscopy (UPS) or photoelectron spectroscopy in air (PESA),[24] with the latter being used in this work. The I_p of the synthesized materials was determined through the measurements on a material drop-casted on a glass substrate. More detailed information can be found in the SI.

The I_p values of the **2PACz** derivatives with phenyl, methyl, and methoxy functional groups range between 5.16 and 5.66 eV. The values obtained for the **3,6-MeO-2PACz** molecule are in good agreement with previously published results.[15] All the corresponding values are given in Table 1. Substitution patterns in all cases suggest that the lowest values were obtained for 3,6 substituted materials (**3,6-Ph-2PACz**, **3,6-Me-2PACz**, and **3,6-MeO-2PACz**). Also, all the 2,7-substituted materials exhibited higher I_p values than the 3,6-substituted compounds. The relatively broad coverage of the I_p values makes this set of materials valuable for further investigation.

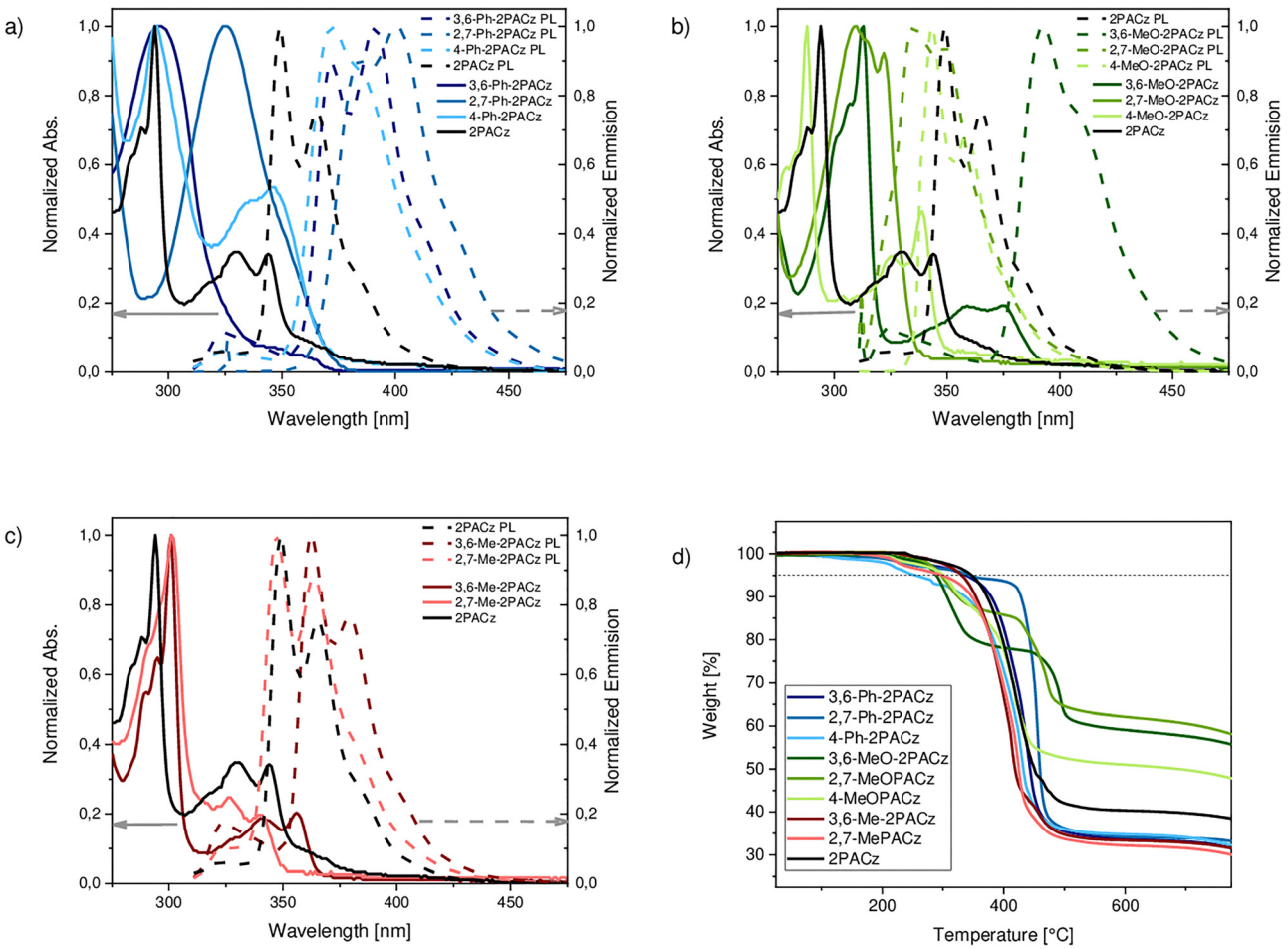

Fig. 3 UV-Vis absorption (solid line) and photoluminescence (dashed line) spectra of materials in tetrahydrofuran (THF) solution (10^{-4} M) of (a) Ph-series, (b) MeO-series, (c) 2PACz derivatives with methyl substituents (Me-series); (d) thermogravimetric analysis (TGA) data (heating rate of 10 °C min^1, N_2 atmosphere).

Table 1 Ionization potential (I_p) values, determined *via* PESA, work functions (WF) determined *via* KPFM, and DFT-calculated values for the lowest-energy rotamer of the investigated compounds

Material	Ip [eV]	WF [eV]	Dipole moment [D]
3,6-Ph-2PACz	5.41	4.98	2.41
2,7-Ph-2PACz	5.54	4.73	1.72
4-Ph-2PACz	5.66	4.93	1.85
3,6-MeO-2PACz	5.16	4.75	2.76[a]
2,7-MeO-2PACz	5.37	4.61	4.20[a]
4-MeO-2PACz	5.20	4.53	1.46
3,6-Me-2PACz	5.30	4.61	1.59
2,7-Me-2PACz	5.47	4.97	2.05
2PACz	5.65	5.28	1.92
ITO		4.40	

[a] For 3,6-MeO-2PACz and 2,7-MeO-2PACz, there are rotamers with close energy values (see Table S3).

The SAMs are known for their tunable dipole moment dependent on the functional group selection and their position in the chromophore, which can impact the work function. To determine the dipole moments of the SAM material, density functional theory (DFT) calculations were conducted on various PACz derivative chromophores. Based on the assumption that the dipole moment in this series is governed by the substituted carbazole head group (the linker and anchoring fragment being the same), and to avoid complications due to the rotamers of the phosphonic acid group, simplified structures were used with the $-CH_3$ fragment at 9*H* position.

The obtained values for the **2PACz** and **3,6-MeO-2PACz** chromophores are in good agreement with previously published results.[3,15] For the Me-series, the calculated dipole moment for the molecule with 3,6 methyl substituents is lower. On the other hand, methyl groups in 2,7 positions result in a dipole moment similar to the one of **2PACz**. All relevant information is provided in the SI (Table S3), and the dipole moments of the lowest energy rotamers are listed in Table 1.

For materials with phenyl rings placed in the 3,6-positions of the carbazole, the calculated dipole moment is higher. Conversely, with substituents in the 2,7- and 4-positions, the

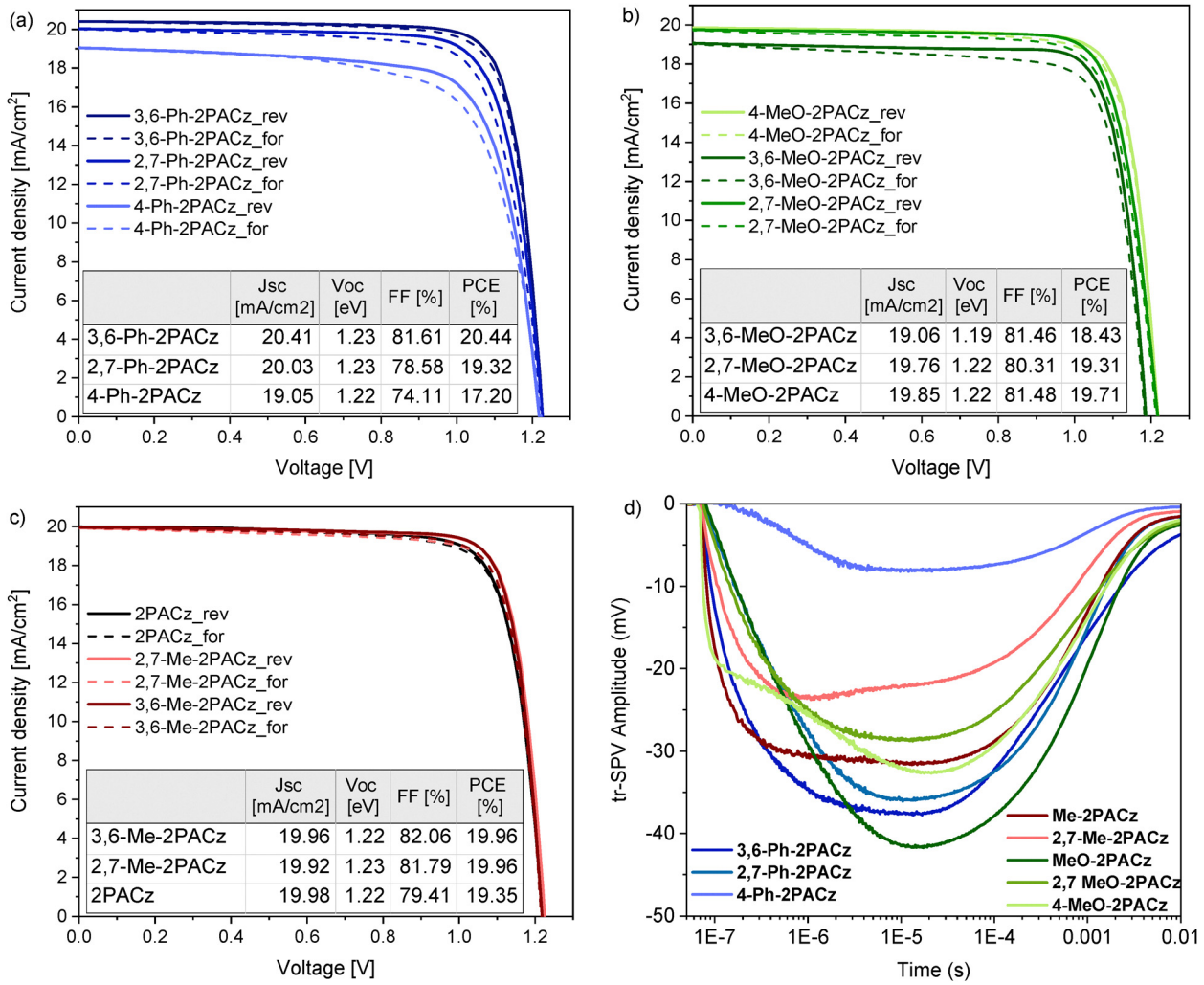

Fig. 4 (a) *J*–*V* characteristics of the devices with Ph-series materials; (b) with MeO-series; (c) with Me-series and 2PACz; (d) tr-SPV of solar cell partial stacks (glass/ITO/SAM/perovskite). SAM powder for the SAM layer was dissolved in ethanol (concentration of the solution 1 mmol l^{-1}). Rev – reverse scan; for – forward scan. In the table values of the reverse scan are presented.

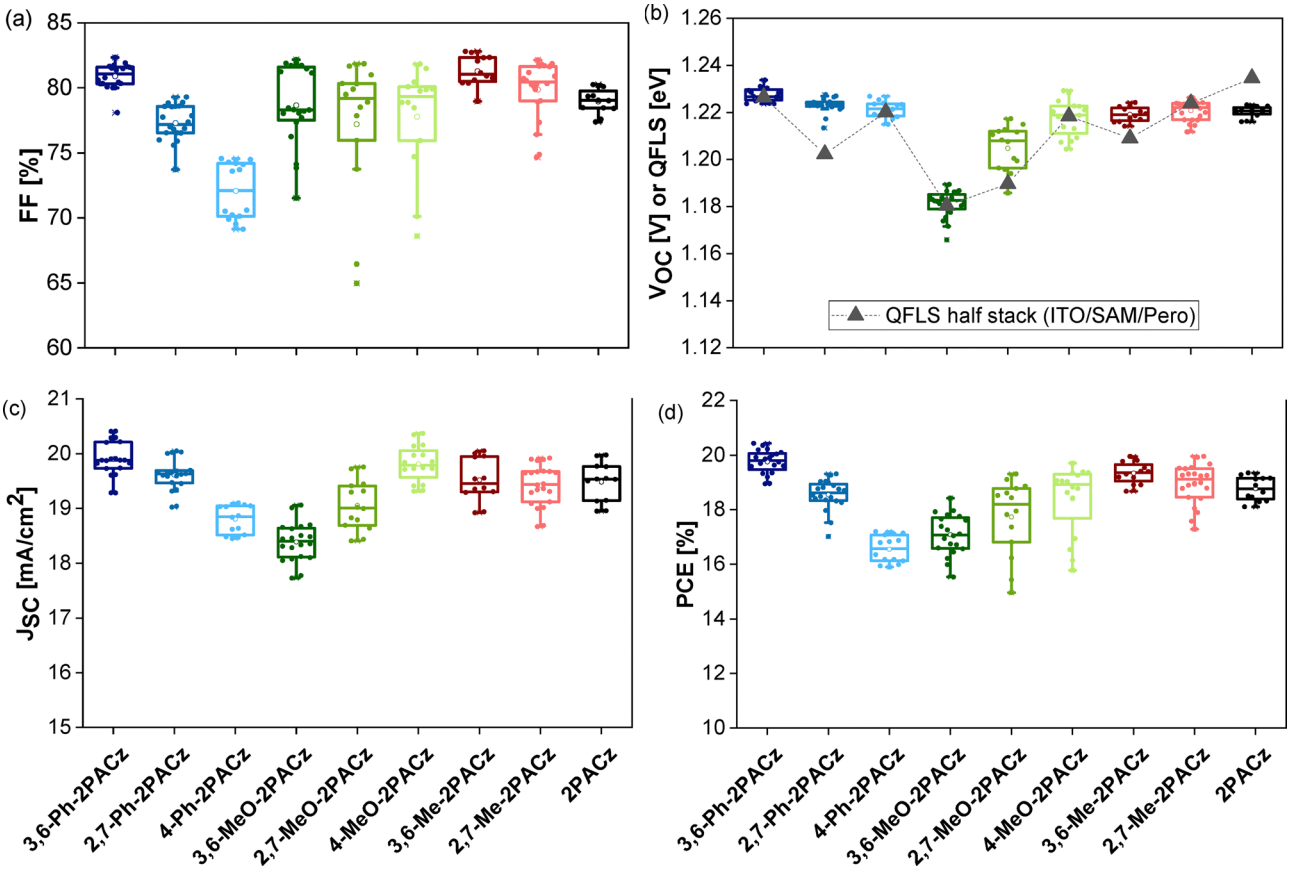

Fig. 5 (a) FF and (b) V_{OC} and QFLS from PL measurements of solar cell partial stacks, (c) J_{SC}, (d) PCE of perovskite single-junction devices.

dipole moment is slightly lower. This can be explained by the conjugation within the molecule, which is greater in the case of 3,6-substitution compared to the other positions. To account for the free rotation around the single bond, in the case of methoxy substituents (**3,6-MeO-2PACz** and **2,7-MeO-2PACz**) we performed calculations of two possible rotamers (SI Table S4).

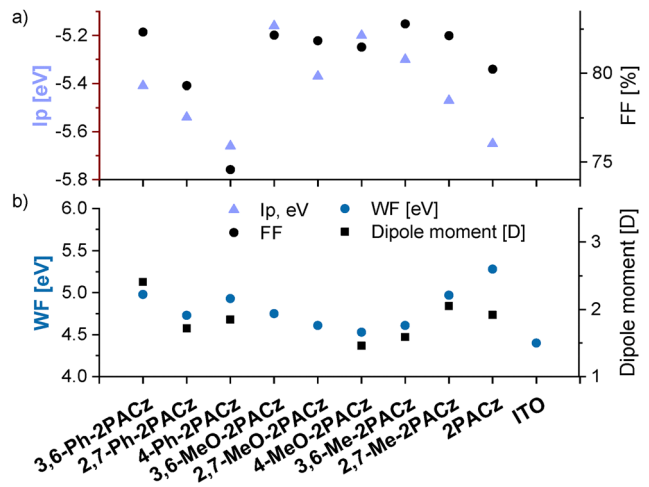

Fig. 6 (a) Ionization potential and fill factors of the devices with given materials. (b) Work function and dipole moments. *Dipole moments are given as a value for the rotamer with the lowest energy.

The obtained values for **3,6-MeO-2PACz** rotamers are consistent with the previous report,[15] and are showing big differences in dipole values. Keeping in mind that the exact distribution between rotamers after assembly on the ITO surface is hard to assess, we have excluded these values from analysis in Fig. 6b.

In recent works, Kelvin probe force microscopy (KPFM) method gained popularity for the characterization of SAM materials, to demonstrate the impact on surface coverage and measure the surface potential and the work function (WF).[25,26] In this work, it was used to evaluate the properties of the investigated materials deposited on ITO. The results are presented in Fig. 6 with the values summarized in Table 1 and Table S3. The KPFM data table illustrates how different **2PACz** derivatives on ITO substrates influence surface potential and work function. The results show a good correlation between the WF and the calculated dipole moment, as can be seen in Fig. 6b. For the molecules with methoxy substituents, the dipole values vary significantly from 0.18 D to 4.20 D for the two rotamers with the lowest energy, making it difficult to use these values for further analysis. Therefore, these values were not included in Fig. 6b.

Solar cell performance

For the screening of the materials, we have used a standard PSC architecture (Glass/ITO/SAM/Perovskite/LiF/C_{60}/SnO_x/Ag),

providing a good baseline protocol. A triple-cation triple-halide perovskite ($Cs_{0.22}FA_{0.78}Pb(Br_{0.15}I_{0.85})_3$ + 5% $MAPbCl_3$) with a 1.68 eV band gap, typically applied in perovskite/Si tandem solar cells,[27,28] was used.

For the device fabrication, we deposited the SAM materials *via* spin-coating on ITO substrates (1 mmol ml^{-1} in ethanol) followed by the deposition of the perovskite. Next, 1 nm of LiF and 16 nm of C_{60} were deposited by thermal evaporation, followed by the deposition of 10 nm SnO_x *via* atomic layer deposition (ALD) and 100 nm thermally evaporated Ag. A detailed description of the device fabrication is provided in the SI.

First, we compare the variation in the fill factor (FF) (Fig. 4a and 5). It can be observed that for all the materials the FF (of the best pixel) is higher for the 3,6-substitution case, with the most pronounced effect being for the molecules with the phenyl substituents (Ph-series: **3,6-Ph-2PACz**, **2,7-Ph-2PACz**, **4-Ph-2PACz**). The low FF, as well as reduced J_{SC} for the devices made utilizing **4-Ph-2PACz** and **2,7-Ph-2PACz** molecules could be related to an extraction barrier for holes at the perovskite/hole transporting layer (HTL) interface as further supported by trSPV (transient surface photovoltage) measurements and PESA measurements. As can be seen from Fig. 6a, after a certain threshold ($I_p > \sim 5.45$ eV), the FF starts to drop, suggesting the suboptimal band alignment. In comparison with the Ph-series, FF changes of the compounds with methoxy substituents (MeO-series) are minor. However, we see distinct changes in the open-circuit voltage (V_{OC}) when changing the position of the MeO-groups on the carbazole body with the lowest V_{OC} for **3,6-MeO-2PACz** and the highest V_{OC} with **4-MeO-2PACz** (Fig. 4b). A lower V_{OC} could be related to increased non-radiative recombination at the interface.

Although not as pronounced as for the Ph-series, also in the Me-series, we observed a higher FF when the functional groups were located at the 3,6-position compared to the 2,7-positions. Moreover, all devices with SAM materials which have functional groups in 3,6 positions and the case of the Me-series and MeO-series, also the 2,7-positions, show a higher FF than the widely applied **2PACz**. The presented comparison confirms the superiority of several compounds, in comparison to the basic compound **2PACz**. In particular, already known materials with substituents in 3,6 positions have shown higher performance, mainly due to the higher FF. In addition, the new materials **2,7-Me-2PACz** and **4-MeO-2PACz** also result in an improved performance in comparison to standard **2PACz**.

The observed trends are further supported by photoluminescence (PL) and trSPV measurements.

As depicted in Fig. 4b the quasi-Fermi level splitting (QFLS) values from steady-state absolute PL measurements of the half stack (Glass/ITO/SAM/Perovskite) largely match the V_{OC} trends of the complete devices.

The trSPV data of solar cell partial stacks (Glass/ITO/SAM/Perovskite) shown in Fig. 4d reveal a relatively small slope for the initial SPV transient with the SAM molecules **4-Ph-2PACz**, **2,7-Ph-2PACz** and **2PACz**, which matches the lower FF that was observed in the complete devices. Such behavior in trSPV was previously correlated with a reduced hole transfer rate.[29] The small SPV amplitude with **4-Ph-2PACz** further points to a small number of extracted holes and, thus, matches the assumption of a barrier for holes at the perovskite/HTL interface. Moreover, **3,6-Me-2PACz**, **3,6-Ph-2PACz**, and **2PACz** show the largest amplitude which is indicative of efficient charge separation and reduced electron trapping.

In addition, we have looked for the correlation between Ip results and the FF of the devices (Fig. 6a). While it is difficult to account for the minor changes, it can be assumed that after a certain threshold I_p value of ~ 5.45 eV the FF starts to drop below 81%.

Conclusions

In conclusion, we made a direct comparison of a set of nine different molecules of hole-selective self-assembled monolayers, which were tested in p–i–n perovskite solar cells using a 1.68 eV bandgap absorber. In this set, five of the molecules were previously published and four were newly synthesized, with phenyl (**3,6-Ph-2PACz**, **2,7-Ph-2PACz**, **4-Ph-2PACz**), methoxy (**3,6-MeO-2PACz**, **2,7-Me-2PACz**, **4-MeO-2PACz**), methyl functional groups (**3,6-Me-2PACz**, **2,7-Me-2PACz**) and 2PACz. A comparison of the various substitution patterns revealed that the highest fill factor of the device was achieved for the materials with substituents in 3,6 positions, independent of the substituent which also correlates with trSPV results. In addition, the PESA measurements suggest a threshold Ip value of ~ 5.45 eV, after which the FF starts to drop. The devices with **4-Ph-2PACz** exhibit the lowest efficiency, due to poor charge extraction as confirmed by trSPV. Additionally, devices with methyl substituents, **4-MeO-2PACz**, **2,7-MeO-2PACz**, **3,6-Ph-2PACz**, and **2,7-Ph-2PACz**, showed higher efficiency results than **2PACz**, demonstrating the impact of the small changes in the molecular structures. While the final performance of the device depends on a combination of the materials, we believe that this study will contribute to the further development of phosphonic acid-based materials and highlight the importance of understanding SAM's working mechanisms at a deeper level.

Conflicts of interest

There are no conflicts to declare.

Data availability

The data supporting this article, including synthesis and methods details, NMR data have been included as part of the supplementary information (SI). See DOI: **https://doi.org/10.1039/d5ma00703h**.

Acknowledgements

A. M. and A. D. acknowledge funding received from the Research Council of Lithuania (LMTLT), agreement No S-MIP-23-92.

A. M. and A. D. would like to thank Egidijus Kamarauskas and Ernestas Kasparavičius for their help in the determination of energy levels. S. A., I. T., E. K. and L. Z. acknowledge funding from the Helmholtz Association within the HySPRINT Innovation lab project and the project ''Zeitenwende–Zukunftstechnologie Tandem–Solarzellen'', the HyPerCells research school and. S. A. and I. T. acknowledge Deutsche Forschungsgemeinschaft (DFG, German Research Foundation) for funding project 424709669 – SPP 2169 (HIPSTER-PRO).

References

1 P. Zhu, C. Chen, J. Dai, Y. Zhang, R. Mao, S. Chen, J. Huang and J. Zhu, *Adv. Mater.*, 2024, **36**(15), 2307357.
2 A. Magomedov, A. Al-Ashouri, E. Kasparavičius, S. Strazdaite, G. Niaura, M. Jošt, T. Malinauskas, S. Albrecht and V. Getautis, *Adv. Energy Mater.*, 2018, **8**(32), 1801892.
3 A. Al-Ashouri, A. Magomedov, M. Roß, M. Jošt, M. Talaikis, G. Chistiakova, T. Bertram, J. A. Márquez, E. Köhnen, E. Kasparavičius, S. Levcenco, L. Gil-Escrig, C. J. Hages, R. Schlatmann, B. Rech, T. Malinauskas, T. Unold, C. A. Kaufmann, L. Korte, G. Niaura, V. Getautis and S. Albrecht, *Energy Environ. Sci.*, 2019, **12**, 3356–3369.
4 S. Mariotti, E. Köhnen, F. Scheler, K. Sveinbjörnsson, L. Zimmermann, M. Piot, F. Yang, B. Li, J. Warby, A. Musiienko, D. Menzel, F. Lang, S. Keßler, I. Levine, D. Mantione, A. Al-Ashouri, M. S. Härtel, K. Xu, A. Cruz, J. Kurpiers, P. Wagner, H. Köbler, J. Li, A. Magomedov, D. Mecerreyes, E. Unger, A. Abate, M. Stolterfoht, B. Stannowski, R. Schlatmann, L. Korte and S. Albrecht, *Science*, 2023, **381**, 63–69.
5 X. Y. Chin, D. Turkay, J. A. Steele, S. Tabean, S. Eswara, M. Mensi, P. Fiala, C. M. Wolff, A. Paracchino, K. Artuk, D. Jacobs, Q. Guesnay, F. Sahli, G. Andreatta, M. Boccard, Q. Jeangros and C. Ballif, *Science*, 2023, **381**, 59–63.
6 E. Aydin, E. Ugur, B. K. Yildirim, T. G. Allen, P. Dally, A. Razzaq, F. Cao, L. Xu, B. Vishal, A. Yazmaciyan, A. A. Said, S. Zhumagali, R. Azmi, M. Babics, A. Fell, C. Xiao and S. De Wolf, *Nature*, 2023, **623**, 732–738.
7 A. Al-Ashouri, E. Köhnen, B. Li, A. Magomedov, H. Hempel, P. Caprioglio, J. A. Márquez, A. B. Morales Vilches, E. Kasparavicius, J. A. Smith, N. Phung, D. Menzel, M. Grischek, L. Kegelmann, D. Skroblin, C. Gollwitzer, T. Malinauskas, M. Jošt, G. Matič, B. Rech, R. Schlatmann, M. Topič, L. Korte, A. Abate, B. Stannowski, D. Neher, M. Stolterfoht, T. Unold, V. Getautis and S. Albrecht, *Science*, 2020, **370**, 1300–1309.
8 H. Chen, C. Liu, J. Xu, A. Maxwell, W. Zhou, Y. Yang, Q. Zhou, A. S. R. Bati, H. Wan, Z. Wang, L. Zeng, J. Wang, P. Serles, Y. Liu, S. Teale, Y. Liu, M. I. Saidaminov, M. Li, N. Rolston, S. Hoogland, T. Filleter, M. G. Kanatzidis, B. Chen, Z. Ning and E. H. Sargent, *Science*, 2024, **384**, 189–193.
9 J. Suo, B. Yang, D. Bogachuk, G. Boschloo and A. Hagfeldt, *Adv. Energy Mater.*, 2025, **15**(2), 2400205.
10 E. Li, C. Liu, H. Lin, X. Xu, S. Liu, S. Zhang, M. Yu, X. Cao, Y. Wu and W. Zhu, *Adv. Funct. Mater.*, 2021, **31**(35), 2103847.
11 E. Aydin, E. Ugur, B. K. Yildirim, T. G. Allen, P. Dally, A. Razzaq, F. Cao, L. Xu, B. Vishal, A. Yazmaciyan, A. A. Said, S. Zhumagali, R. Azmi, M. Babics, A. Fell, C. Xiao and S. De Wolf, *Nature*, 2023, **623**, 732–738.
12 M. Jošt, E. Köhnen, A. Al-Ashouri, T. Bertram, Š. Tomšič, A. Magomedov, E. Kasparavicius, T. Kodalle, B. Lipovšek, V. Getautis, R. Schlatmann, C. A. Kaufmann, S. Albrecht and M. Topič, *ACS Energy Lett.*, 2022, **7**, 1298–1307.
13 P. J. Hotchkiss, S. C. Jones, S. A. Paniagua, A. Sharma, B. Kippelen, N. R. Armstrong and S. R. Marder, *Acc. Chem. Res.*, 2012, **45**, 337–346.
14 C. E. Puerto Galvis, D. A. González Ruiz, E. Martínez-Ferrero and E. Palomares, *Chem. Sci.*, 2024, **15**, 1534–1556.
15 Y. Lin, A. Magomedov, Y. Firdaus, D. Kaltsas, A. El-Labban, H. Faber, D. R. Naphade, E. Yengel, X. Zheng, E. Yarali, N. Chaturvedi, K. Loganathan, D. Gkeka, S. H. AlShammari, O. M. Bakr, F. Laquai, L. Tsetseris, V. Getautis and T. D. Anthopoulos, *ChemSusChem*, 2021, **14**, 3569–3578.
16 X. Deng, F. Qi, F. Li, S. Wu, F. R. Lin, Z. Zhang, Z. Guan, Z. Yang, C. Lee and A. K.-Y. Jen, *Angew. Chem., Int. Ed.*, 2022, **134**(30), e202203088.
17 G. Wang, J. Zheng, W. Duan, J. Yang, M. A. Mahmud, Q. Lian, S. Tang, C. Liao, J. Bing, J. Yi, T. L. Leung, X. Cui, H. Chen, F. Jiang, Y. Huang, A. Lambertz, M. Jankovec, M. Topič, S. Bremner, Y.-Z. Zhang, C. Cheng, K. Ding and A. Ho-Baillie, *Joule*, 2023, **7**, 2583–2594.
18 A. Al-Ashouri, E. Köhnen, B. Li, A. Magomedov, H. Hempel, P. Caprioglio, J. A. Márquez, A. B. Morales Vilches, E. Kasparavicius, J. A. Smith, N. Phung, D. Menzel, M. Grischek, L. Kegelmann, D. Skroblin, C. Gollwitzer, T. Malinauskas, M. Jošt, G. Matič, B. Rech, R. Schlatmann, M. Topič, L. Korte, A. Abate, B. Stannowski, D. Neher, M. Stolterfoht, T. Unold, V. Getautis and S. Albrecht, *Science*, 2020, **370**, 1300–1309.
19 Q. Chen, K. Sun, L. R. Franco, J. Wu, L. Öhrström, X. Liu, M. Gumbo, M. S. Ozório, C. M. Araujo, G. Zhang, A. Johansson, E. Moons, M. Fahlman, D. Yu, Y. Wang and E. Wang, *Adv. Sci.*, 2025, **12**(4), 2410277.
20 G. Li, Z. Su, L. Canil, D. Hughes, M. H. Aldamasy, J. Dagar, S. Trofimov, L. Wang, W. Zuo, J. J. Jerónimo-Rendon, M. M. Byranvand, C. Wang, R. Zhu, Z. Zhang, F. Yang, G. Nasti, B. Naydenov, W. C. Tsoi, Z. Li, X. Gao, Z. Wang, Y. Jia, E. Unger, M. Saliba, M. Li and A. Abate, *Science*, 2023, **379**, 399–403.
21 Q. Jiang, J. Tong, Y. Xian, R. A. Kerner, S. P. Dunfield, C. Xiao, R. A. Scheidt, D. Kuciauskas, X. Wang, M. P. Hautzinger, R. Tirawat, M. C. Beard, D. P. Fenning, J. J. Berry, B. W. Larson, Y. Yan and K. Zhu, *Nature*, 2022, **611**, 278–283.
22 R. Chen, Y. Hui, B. Wu, Y. Wang, X. Huang, Z. Xu, P. Ruan, W. Zhang, F. Cheng, W. Zhang, J. Yin, J. Li and N. Zheng, *J. Mater. Chem. A*, 2020, **8**, 9597–9606.
23 O. Perez, C. Bloyet, J.-M. Rueff, N. Barrier, V. Caignaert, P.-A. Jaffrès and B. Raveau, *Cryst. Growth Des.*, 2016, **16**, 6781–6789.

24 J. Bertrandie, J. Han, C. S. P. De Castro, E. Yengel, J. Gorenflot, T. Anthopoulos, F. Laquai, A. Sharma and D. Baran, *Adv. Mater.*, 2022, **34**(35), 2202575.
25 F. J. Angus, W. K. Yiu, H. Mo, T. L. Leung, M. U. Ali, Y. Li, J. Wang, A. W. Y. Ho-Baillie, G. Cooke, A. B. Djurišić and P. Docampo, *J. Phys. Chem. Lett.*, 2024, **15**, 10686–10695.
26 T. Hellmann, C. Das, T. Abzieher, J. A. Schwenzer, M. Wussler, R. Dachauer, U. W. Paetzold, W. Jaegermann and T. Mayer, *Adv. Energy Mater.*, 2020, **10**(42), 2002129.
27 S. Mariotti, E. Köhnen, F. Scheler, K. Sveinbjörnsson, L. Zimmermann, M. Piot, F. Yang, B. Li, J. Warby, A. Musiienko, D. Menzel, F. Lang, S. Keßler, I. Levine, D. Mantione, A. Al-Ashouri, M. S. Härtel, K. Xu, A. Cruz, J. Kurpiers, P. Wagner, H. Köbler, J. Li, A. Magomedov, D. Mecerreyes, E. Unger, A. Abate, M. Stolterfoht, B. Stannowski, R. Schlatmann, L. Korte and S. Albrecht, *Science*, 2023, **381**, 63–69.
28 J. Xu, C. C. Boyd, Z. J. Yu, A. F. Palmstrom, D. J. Witter, B. W. Larson, R. M. France, J. Werner, S. P. Harvey, E. J. Wolf, W. Weigand, S. Manzoor, M. F. A. M. van Hest, J. J. Berry, J. M. Luther, Z. C. Holman and M. D. McGehee, *Science*, 2020, **367**, 1097–1104.
29 I. Levine, A. Al-Ashouri, A. Musiienko, H. Hempel, A. Magomedov, A. Drevilkauskaite, V. Getautis, D. Menzel, K. Hinrichs, T. Unold, S. Albrecht and T. Dittrich, *Joule*, 2021, **5**, 2915–2933.